

Response of the Verwey transition in magnetite to a controlled point-like disorder induced by 2.5 MeV electron irradiation

Ruslan Prozorov,^{1,2,*} Makariy A. Tanatar,^{1,2} Erik I. Timmons,^{1,2} Marcin Kończykowski,³ and Tanya Prozorov^{1,4}

¹*Ames National Laboratory, Ames, Iowa 50011, USA*

²*Department of Physics & Astronomy, Iowa State University, Ames, Iowa 50011, USA*

³*Laboratoire des Solides Irradiés, École Polytechnique, CNRS,*

CEA, Institut Polytechnique de Paris, F-91128 Palaiseau, France

⁴*Department of Chemical and Biological Engineering, Iowa State University, Ames, Iowa 50011, USA*

(Dated: 14 May 2023)

A controlled point-like disorder induced by low temperature 2.5 MeV electron irradiation was used to probe the nature of the Verwey transition in magnetite, Fe_3O_4 . Two large single crystals, one with optimal transition temperature, $T_V \approx 121$ K, and another with $T_V \approx 109$ K, as well as biogenic nanocrystals, $T_V \approx 110$ K, were examined. Temperature-dependent resistivity is consistent with the semiconductor-to-semiconductor sharp, step-like Verwey transition from a state with a small bandgap of around 60 meV to a state with a larger bandgap of about 300 meV. The irradiation causes an up-shift of the resistivity curves above the transition without transition smearing or broadening. It also causes an apparent down-shift of the resistivity maximum at high temperatures. In the lower T_V crystal, the electron irradiation drives the transition temperature into a “forbidden” regime believed to separate the first order from the second order phase transition. Contrary to this belief, the transition itself remains sharp and hysteretic without a significant change in the hysteresis width. We conclude that the sudden change of the bandgap accompanied by the monoclinic distortion and the change of magnetic anisotropy is the reason for the Verwey transition in magnetite and the effect of additional disorder is mostly in the smearing of the sharp gap edges near the Fermi level.

I. INTRODUCTION

The original studies of magnetite, Fe_3O_4 , have initiated one of the most fascinating topics in condensed matter physics, the metal-insulator transition (MIT) [1–3]. (Although now we know that, specifically in magnetite, the transition is a semiconductor-to-semiconductor type [4]). It all started in 1926 when an unexpected heat absorption at around 115 K - 117 K was found in heat capacity measurements by Parks and Kelley [1]. The authors write: “The heat absorption, found in the case of the magnetite crystals at about 115 K, constitutes still another noteworthy feature. This temperature would seem to be very low for a transformation in crystal structure in a metallic oxide, the melting-point of which is above 1500 K. ... we think that the observed heat effect may possibly be connected with a change in the magnetic properties of the substance. ... Certainly this heat absorption phenomenon should be investigated further.” No graphics/figures were shown, though in Ref.[1]. Next, magnetic anomalies at similar temperatures were reported [5, 6], seemingly agreeing with the assumption of the magnetic origin of the observed behavior because no difference was found in x-ray diffraction measured at room temperature and at liquid “air” (nitrogen) [6]. Finally, thirteen years after the initial work, Verwey reported now famous two orders of magnitude sharp increase of resistivity at around 120 K [2, 3]. Since that time, it became known as the “Verwey transition,” and

its microscopic origins have been a subject of relentless experimental and theoretical research to this day. Here we can only mention a very incomplete set of review articles [7–20].

Stoichiometric magnetite is a mix of iron oxides, $\text{Fe}_3\text{O}_4 = \text{Fe}_2^{3+}\text{O}_3^{2-} \cdot \text{Fe}^{2+}\text{O}^{2-}$, which has an inverse spinel crystal structure with iron ions occupying two distinct sites, $\text{Fe}_3\text{O}_4 = [\text{Fe}^{3+}(\text{A}) + \text{Fe}^{3+}\text{Fe}^{2+}(\text{B})] \cdot \text{O}_4$ where A sites are coordinated in a tetrahedron and B sites are coordinated in an octahedron. Ionic magnetic moments at the A and B sites are antiparallel, resulting in ferrimagnetism with an excess magnetic moment of about $4\mu_B$ per formula units (f.u.). For each formula unit, there are two B sites with spin $S = 2.25\mu_B$ and one A site with $S = 2.5\mu_B$. There are 8 f.u. in a deformed cubic cell with lattice constant of $a = 8.4 \text{ \AA}$, so each cubic unit cell contributes $32\mu_B$ of net moment. Magnetite’s Curie temperature is about 800 K [21]. Above the Verwey transition temperature, $T_V \approx 121$ K, the B sites are charge-frustrated leading to a significant delocalization of electrons, which results in a moderately conducting state with the resistivity of about $0.005 - 0.01 \Omega \cdot \text{cm}$ at room temperature and about $0.02 \Omega \cdot \text{cm}$ at T_V . Verwey discovered that below T_V , the resistivity increases sharply by about two orders of magnitude and continues to increase significantly upon further cooling. He has explained this behavior in terms of charge ordering in the B subsystem: Fe^{2+} ions along the $[110]$ and Fe^{3+} along $[1\bar{1}0]$ directions. This is called a “Verwey model” [2, 3, 9]. The resistive and thermodynamic signatures of the Verwey transition are accompanied by the step-like change in sample magnetization and all other thermodynamic, spectroscopic and transport properties [9]. Simi-

* Corresponding author: prozorov@ameslab.gov

lar to the resistive Verwey transition, the physics of the magnetic anomaly apparently associated with it, is still debatable. It is known that magnetic easy axis changes from the [111] to [100] (within 0.2 \AA due to small monoclinic distortion) direction below T_V . The K_1 term of magnetic anisotropy energy increases by an order of magnitude, but the amplitude of the total magnetic moment remains unchanged.

Since the original proposal, different mechanisms of the Verwey transition considering new experimental results have been put forward. Resonant X-ray studies found no evidence of charge ordering and strong electron-phonon interaction was suggested as the cause of the Verwey transition [22]. Anderson argued that in spinel's octahedral sites, nearest-neighbor Coulomb interactions can never lead to the long-range order, and even the long-range Coulomb interaction are practically ineffective at least at higher temperatures [23]. Based on the large thermopower and low conductivity observed in magnetite both below and above the Verwey transition, it was suggested that Anderson localization due to randomness of electrons and impurities is involved [24–26]. In general, some form of electron localization (e.g., trimerons [27–32]) is considered as one of the primary mechanisms of the transition. It was also demonstrated that the collective Jahn-Teller distortion due to interacting local degeneracies may play an important role [28, 33–35]. It supports some other ideas, such as the cooperative ordering of molecular polarons below T_V [36]. From another angle, Mott suggested that the Verwey transition is a transition from Wigner glass to Wigner crystal in an electronic subsystem, but there was not much of experimental followup [37, 38]. Considering non-metallic behavior, it was also suggested that the condensation of active optical phonon mode could be the reason for the transition [39] and it seems that the oxygen-18 isotope effect study supported it [40].

On the opposite side from electron localization mechanisms, there is overwhelming experimental and theoretical evidence for the fairly large ($\sim 200 \text{ meV}$) bandgap opening below the Verwey temperature [4, 16, 18, 41, 42]. This gap could originate from the charge-orbital ordering due to the on-site Coulomb interactions [43]. Yet, some details are not quite clear. Some studies assert that the energy gap only opens below T_V , while above the transition the electronic bandstructure is gapless and involves molecular polarons hopping conductivity [16, 18, 42]. Scanning tunneling spectroscopy (STS) shows directly a clear smaller gap, of the order of 70 meV , above T_V transition and a larger gap below [4, 41]. Diffusive x-ray scattering study finds short-range charge ordering above T_V related to trimeron ordering below the transition. This short-range ordering persist at least up to room temperature and is, apparently, correlated with the Fermi surface nesting signatures [32], which again would imply opening the small energy gaps at least on parts of the Fermi surface.

Another experimental puzzle in magnetite is the dis-

continuity of the Verwey transition separating first order phase transition in relatively clean compositions from the (alleged) second order transition in less stoichiometric compounds. For example, in $\text{Fe}_{3(1-\delta)}\text{O}_4$, the critical value of $\delta_c = 0.0039$ [10, 44–48]. Ironically, the temperature-dependent resistivity in the latter regime is highly hysteretic, pointing to a first-order nature of the transition. No satisfactory explanation for this disparity exists [10, 46, 49]. Similar bifurcation was observed in chemically substituted magnetite, $\text{Fe}_{3(1-x)}\text{M}_{3x}\text{O}_4$, with $\text{M} = \text{Ni}, \text{Co}, \text{Mg}, \text{Al}, \text{Ti}, \text{Mn}, \text{Li}$ (sorted from the lowest to the highest rate of T_V suppression) [50–53]. In this work, we show that the Verwey transition continues to remain first order when driven to the “forbidden” range of T_V values by disorder. It shows that off-stoichiometry and disorder are not equivalent.

The measurements under applied isostatic or directional (uniaxial strain) pressure support this assertion. Isostatic pressure suppresses the Verwey temperature and, at around a critical value of $P_c \approx 8 \text{ GPa}$, recovers the higher-conductance “metallic” state, although the details of P_c and other features vary between different studies [16, 47, 54–56]. Directional stress leads to the enhancement of T_V , most likely due to favorable structural domain selectivity [17, 21, 57]. In either case, pressure/strain change T_V continuously (but at P_c it disappears abruptly) and the significant hysteresis in the measured quantity is observed, supporting our statement above.

Finally, another line of study was inspired by the reports of a significant smearing and shifting of the Verwey transition in magnetite nanoparticles of different size with initial reports showing the effect already at about 100 nm , which is quite large for the local-moment magnetism [18, 58–63]. This sub-field of magnetite nanoparticles grew very rapidly and, unfortunately, it is very difficult or mostly impossible to know whether those numerous reports have actually had nanocrystalline magnetite of a mix of iron oxides or just maghemite, $\gamma\text{-Fe}_2\text{O}_3$. Many studies rely on the conventional x-ray diffraction, but at room temperature it is hard to distinguish between different oxides because both have the same cubic structure and their lattice parameters are almost identical [64]. Moreover, it is likely that nanoparticles powder-like samples actually contain different compositions in comparable proportions [64]. The only reliable feature, present only in magnetite, the Verwey transition is smeared and broadened in nanoparticles assemblies due to size and shape distributions, stress, strain and the variation of stoichiometry, hence is difficult to identify. The biological magnetite is the exception, as it comes as well-shaped particles of a similar size [65, 66] and is proven to be Fe_3O_4 by the magnetic induction mapping using electron holography [67, 68] and NV-centers in diamond [69]). One of the most detailed systematic investigations where a great deal of attention was devoted to the identification of magnetite as the primary phase, expectantly showed that the Verwey transition remains

practically unchanged down to a nanoparticle size of 8 nm, below which T_V drops very rapidly [70]. Similar conclusions were drawn by considering biological magnetite of magneto-tactic bacteria where the chemical composition is preserved by the lipid membranes preventing oxidation [66]. Of course, an additional technical problem is the size-dependent superparamagnetic nature of magnetite nanoparticles [61, 66, 71, 72]. The magnetic signature of the Verwey transition measured in nanoparticle assemblies is smeared simply because of the size-dependent blocking temperature, T_B , which quickly becomes lower than bulk T_V rendering magnetic signature of the Verwey transition ill-defined, while direct transport measurements on single nanoparticles are not generally possible in most labs. In case of fairly large (50 nm) biological nanoparticles, the Verwey transition is somewhat smeared, yet, it is quite well-defined because blocking temperature is close to room temperature [66] (also, see the data below).

With so much experimental and theoretical effort devoted to magnetite and the Verwey transition over almost 100 years, what new can one possibly do and find? In order to shed some more light on this fascinating topic, we used a controlled point-like disorder as a probe. We stress that chemical doping or intentional variation of Fe/O ratio conducted in many works in the past, is not equivalent to the artificial uncorrelated disorder, because such disorder does not “dope” the system and does not change the Fermi energy. (This was checked using Hall effect measurements on pristine and disordered samples, albeit in a different system [72].) If Verwey’s charge ordering, Anderson localization, or the formation of Wigner crystal scenarios were realized, we would expect to observe a substantial smearing of the transition upon the introduction of random disorder. In the case of polarons, it is unclear what to expect with the added disorder. If, on the other hand, the disorder only affects the bandwidth and/or introduces the extra “impurity” band, the transition temperature, T_V , would shift to the lower temperature, because the clean band-gap will become smaller but the transition itself would remain sharp and hysteretic. Unfortunately, we did not find systematic theoretical studies of the possible effects of point-like disorder on the Verwey transition. It was suggested that impurities may lead to closing up the gap above T_V [52, 73]. However, this is not supported by the experiment and the Authors considered an actual ionic substitution rather than dilute scattering centers. Perhaps our work will serve as the motivation for further studies.

II. EXPERIMENTAL

A. Controlled artificial point-like disorder

The point-like disorder was introduced at the SIRIUS facility in the Laboratoire des Solides Irradiés at École Polytechnique, Palaiseau, France. Electrons were accel-

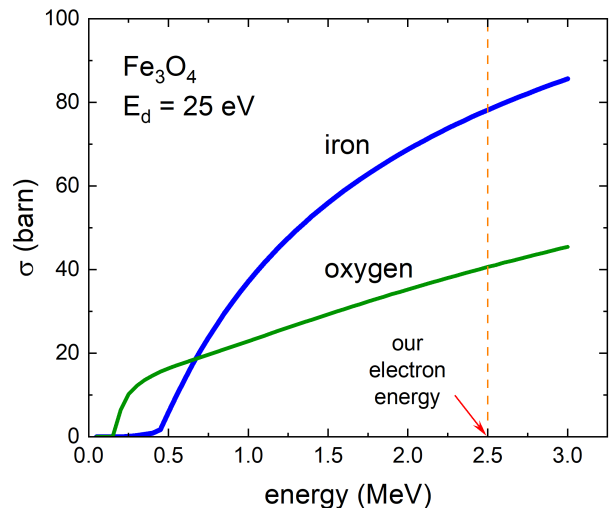


FIG. 1. Partial cross-sections of knock-out defect creation (both, vacancies and interstitials) for iron (blue line) and oxygen (green line) ions in stoichiometric magnetite, Fe_3O_4 , as a function of electron energy assuming the typical displacement energy threshold, $E_d = 25$ eV. At the operating energy of 2.5 MeV, the total cross-section is $\sigma = 56.7$ barn, which leads to the estimate of 2.48×10^{-3} defects per 1 C/cm² per formula unit (*dppf*), Fe_3O_4 .

erated using a pelletron-type linear accelerator to the energy of 2.5 MeV, reaching 0.985 of the speed of light [74]. Such electrons are capable of knocking out ions from crystal lattice creating the so-called Frenkel pairs of vacancy-interstitial [75–79].

Figure 1 shows the ion-type-resolved cross-sections of the defects creation calculated using SECTE (“Sections Efficaces Calcul Transport d’Électrons”) software, developed at École Polytechnique (Palaiseau, France) by members of the “Laboratoire des Solides Irradiés”, specifically for the interpretation of MeV-range electron irradiation using their pelletron-type linear accelerator, SIRIUS [80]. Using atomic weights averages, the SECTE software interpolates the ion knock-out cross-sections tabulated by O. S. Oen [81]. The input parameters are the chemical composition of the substance of interest, the direct head-on knockout energy, $E_d = 25$ eV, and the energy of the projectiles (electrons), 2.5 MeV in our case. We used the commonly assumed value of $E_d = 25$ eV [75, 76] since the exact numbers are unimportant because we are only interested in the order-of-magnitude estimates. We obtained the partial cross-sections, 40.6 barn for oxygen and 78.2 barn for iron. Therefore, the total cross-section is 56.7 barn. With the total beam current, measured behind the sample using a Faraday cage, 2.7 μA through a 5 mm in diameter circular diaphragm, the electron beam flux is 8.6×10^{13} electrons/(s \cdot cm²). The acquired irradiation dose is conveniently measured in C/cm², where 1 C/cm² = 6.24×10^{18} electrons/cm². This gives 3.54×10^{-4} defects per 1 C/cm² per atom (dpa), or 2.48×10^{-3} defects per 1 C/cm² per formula

unit (dpf), Fe_3O_4 (not conventional unit cell with eight formula units!). An interesting feature of Fig.1 is that while at 2.5 MeV iron defects dominate, if the energy is reduced to around 0.5 MeV, the only defects produced will be oxygen interstitials and vacancies. Therefore, it is possible to conduct ion-specific study to determine what kind of defects affect the properties the most.

For the doses used in this work of 2, 3.8, 4.1, and 6.3 C/cm^2 we estimate the concentration of defects to be 5, 9, 10 and 16 defects per thousand of formula units, or 40, 75, 81, 125 defects per thousand of conventional deformed cubic unit cell, or $0.5, 0.9, 1.0, 1.5 \times 10^6$ defects/ cm^3 . These estimates are made under the assumption that all collisions are head-on and there is no recombination of the Frenkel pairs. During electron irradiation, the sample is immersed in liquid hydrogen at around 20 K to remove significant heat of collisions and prevent immediate recombination and clusterization of the defects. On warming to room temperature, the induced defects partially anneal with some Frenkel pairs recombine and ions in interstitial positions migrate to various sinks (dislocations, surfaces etc.) leaving behind a quasi-equilibrium distribution of vacancies which have much higher barrier for diffusion. The resultant level of the induced disorder is reflected in the change of sample resistivity at room temperature where carrier density is roughly constant, and the only change comes from the differences in the residual resistivity before and after irradiation. Typically about 30%-50% of the defects are lost as judged by the in-situ resistivity measurements [77, 78]. For magnetite, such measurement is difficult due to its gapped semiconducting nature.

For comparison, 1% ($\delta = 0.01$) of iron vacancies, $\text{Fe}_{3(1-\delta)}\text{O}_4$, found in biogenic magnetite [12] and synthetic magnetite with different synthesis/annealing protocols [44–46], or ionic substitutions $\text{Fe}_{3(1-x)}\text{M}_{3x}\text{O}_4$, substitutions with $\text{M}=\text{Ni}, \text{Co}, \text{Mg}, \text{Al}, \text{Ti}, \text{Mn}, \text{Li}$ (sorted from lowest to highest rate of T_V suppression) [50–53] corresponds to $dpf = 3\delta/7 = 4.3$ defects per 1000 formula units, comparable with the concentration of defects induced by electron irradiation used in this paper. An important advantage of controlled irradiation is that the same physical sample is studied before and after irradiation without taking off the contacts for transport measurements. This removes any ambiguity that exists when comparing different samples that were subject to different annealing protocols or chemical substitutions.

B. Samples and experimental techniques

Single crystals of Fe_3O_4 were obtained from J. M. Honig, which provided an excellent opportunity to directly compare our measurements before electron irradiation with his published data that were the first published systematic electrical resistivity study of $\text{Fe}_{3-\delta}\text{O}_4$ on a set of samples with different δ . The crystals grown by using the so-called skull melting technique described

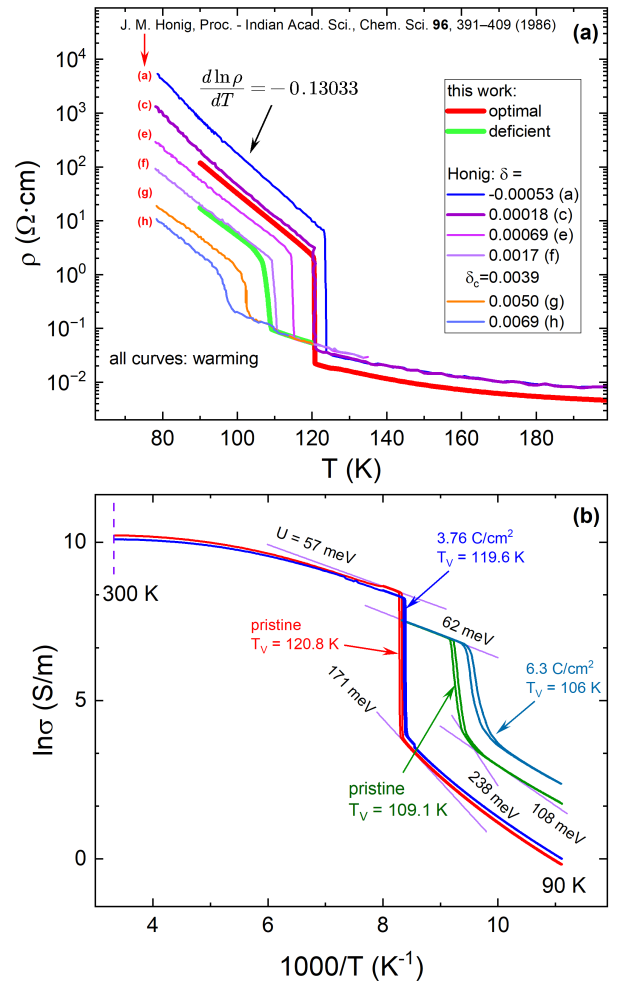


FIG. 2. (a) Temperature-dependent resistivity on a log 10 scale for the samples used in this study, solid red line - optimal, solid green line - oxygen deficient. For reference we plot the data after Honig [46] for oxygen-deficient samples. (b) Arrhenius plots of conductivity, $\ln \sigma$ vs. $1000/T$, for the samples before and after irradiation.

elsewhere [10, 46, 82]. Samples for transport measurements with typical sample sizes of $(1-2) \times 0.3 \times 0.1 \text{ mm}^3$ (length \times width \times thickness) were cut and polished from large single crystals. The short side corresponded to [011] direction.

Electrical transport measurements were performed in a *Quantum Design* physical property measurement system (PPMS) using a standard four-probe method with electrical current flowing along the longer side. The contacts were made by soldering silver wires with indium solder and the follow-up mechanical strengthening with conductive Dupon 4929N silver paste [83]. The contact resistance of these contacts was below $100 \mu\Omega$, and they were mechanically stable to withstand electron irradiation [84]. Importantly, the contacts remained intact between measurements and irradiation runs, thus enabling quantitative characterization of the resistance change without invoking changes in the sample geome-

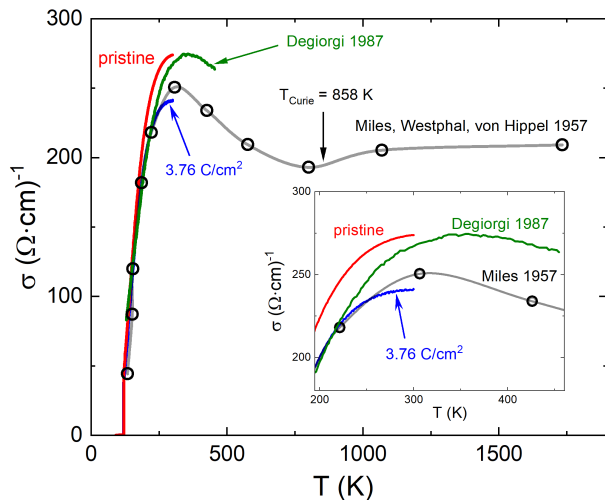


FIG. 3. Electrical conductivity in $(\Omega \cdot \text{cm})^{-1}$ of our pristine magnetite crystal (solid red curve) and irradiated with the dose of 3.76 C/cm^2 (solid blue curve), compared to the literature data up to almost 500 K in Ref. [88] (solid green curve), and extended to much higher temperatures, well above the Curie temperature of 858 K, from Ref. [89], shown by black open circles connected by a gray spline line. The inset focuses on a region of conductivity maximum occurring at around 300 - 350 K.

try.

Magnetite nanocrystals, approximately $20 \times 20 \times 50$ nm in size, were extracted from the lysed cells of magnetotactic bacteria, MV-1 strain [15, 66, 85]. Details of the extraction process and magnetic characterization of different biogenic magnetite strains and single crystals are published elsewhere [66]. The retrieved nanoparticles were smeared on a standard carbon grid for transmission electron microscopy (TEM) studies. For irradiation, the grids were enclosed in thin aluminum pouches for protection. Magnetization measurements were carried out using a *Quantum Design* magnetic property measurement system (MPMS). Magnetite nanocrystals were measured directly before and after irradiation in their aluminum enclosures.

III. RESULTS

We first look at the stoichiometric single crystal and then compare the results with those for off-stoichiometric crystal. The samples for electron irradiation and measurements were cut and shaped from these large crystals as described in the Experimental section. The close to optimal composition crystal had $T_V \approx 121$ K [10, 49], while another had substantially lower $T_V \approx 109$ K, it showed equally sharp transition and thermal hysteresis in $\rho(T)$. For completeness, we also study the effect of disorder on biological magnetite extracted from magnetotactic bacteria [12, 66, 68, 85–87].

Figure 2(a) shows temperature dependent resistivity

on a \log_{10} scale versus temperature for two magnetite single crystals used in this study, with $T_V \approx 121$ K and $T_V \approx 109$ K. For comparison, we re-plot Honig's data from his Fig.13 [46], which was the first systematic reported study of this kind. Remarkably, both below and above T_V , the slopes $d \lg \rho / dT$ are practically identical between all these samples despite the fact that Honig has grouped his samples into groups A (1st order transition) and B (2nd order transition.). In order to examine the thermally activated population of carriers in the conduction band, n_c , Fig. 2(b) presents the natural logarithm of electrical conductivity, $\sigma \sim n_c \sim \exp(-U/T)$ plotted versus $1000/T$. The linear fits around the transition are shown by solid lines in Fig. 2(b). The activation energy, U , is estimated to be about 60 meV above T_V , and about 200 meV just below, regardless of the T_V value, and in a fair agreement with the scanning tunneling spectroscopy (STS) data [41]. In temperature equivalent, these gaps correspond to about 700 K above the transition and 2700 K just below T_V . Above the transition this activation energy corresponds to an energy gap in band-gap model [90], polaron activation energy in the polaron transport model [91], and to energy distance to mobility edge in weak localization model [25].

In Fig. 3 we compare temperature-dependent conductivity σ of high T_V sample (red curve) with previous measurements over extended temperature range, by Degiorgi [88] and by Miles et al. [89]. Similar to these studies, conductivity tends to saturate before reaching a peak at ~ 350 K. A metallic-like decrease of conductivity on heating above the peak may suggest a cross-over to an intrinsic conductivity regime, supporting band transport model [90]. Irradiation with 3.76 C/cm^2 (blue curve), leads to a more pronounced flattening of $\sigma(T)$ curve, suggesting a shift of the maximum to lower temperatures. This may be natural for a semiconductor with higher carrier density, as expected for crystals with higher defect density after irradiation.

Figure 4 presents electrical transport measurements in magnetite single crystal of optimal composition. The black curve is the pristine sample and red is the measurement of a sample after a substantial dose of electron irradiation, $3.76 \text{ C/cm}^2 = 2.3 \times 10^{19} \text{ electrons/cm}^2$ producing a maximum of 9 defects per 1000 formula units. Panel (a) shows $\rho(T)$ on the linear scales. There is a clear signature of the Verwey transition at around 121 K and, as it was first observed by Verwey [2], the resistivity changes by the two orders of magnitude from $0.02 \Omega \cdot \text{cm}$ above T_V to $2 \Omega \cdot \text{cm}$ below. At 90 K, resistivity grows exponentially to $198 \Omega \cdot \text{cm}$. Analysis shown in Fig.2, gives the energy gap for carriers in the conduction band, $U = 171$ meV below T_V and 57 meV above. Panel (b) shows the resistivity plotted on a logarithmic scale zooming in on the Verwey transition region, revealing substantial hysteresis between cooling with its transition temperature, T_V^c , and warming with, $T_V^w > T_V^c$, signaling a strong 1st order phase transition. (Throughout the paper we use higher value, T_V^w , speaking of the

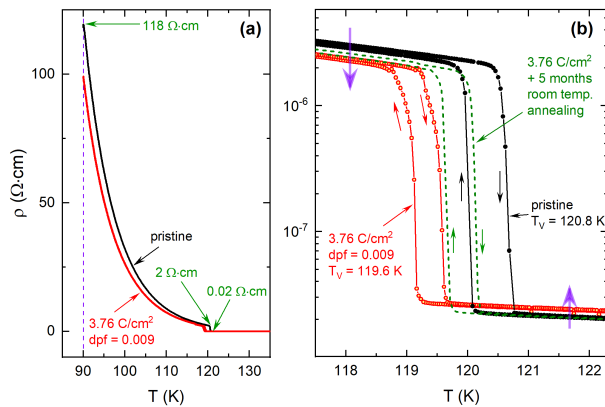


FIG. 4. (a) Temperature-dependent resistivity of optimal single crystal before (black line) and after (red line) electron irradiation with a substantial dose of $3.76 \text{ C/cm}^2 = 2.3 \times 10^{19}$ electrons/cm² producing a maximum of 9 defects per 1000 formula units. There is a clear signature of the Verwey transition at around 121 K where the resistivity changes by two orders of magnitude from $0.02 \Omega \cdot \text{cm}$ above T_V to $2 \Omega \cdot \text{cm}$ below. (b) Resistivity plotted on a logarithmic scale zooming in on the Verwey transition region revealing substantial hysteresis signifying a strong 1st order phase transition. In addition to the curves shown on the left panel, here green dashed line shows the evolution of the Verwey transition after five months of passive room-temperature annealing on the shelf. Importantly, all curves remain parallel at the transition showing no broadening. Also note that irradiation causes an increase of ρ above T_V , and a decrease below as indicated by violet arrows.

generic transition, T_V .) Remarkably, the transition temperature in the irradiated sample shifts by a significant 2.2 K ($\sim 2\%$), but does not smear. All curves remain practically parallel at the transition showing no broadening or smearing. If anything, the hysteresis becomes a little bit smaller. In addition to the curves shown in panel(a), the green dashed line in panel (b) shows the evolution of the Verwey transition after five months of passive room-temperature annealing on the shelf.

Let us switch to an off-stoichiometric magnetite crystal with $T_V \approx 109.1 \text{ K}$. Figure 5 shows measurements similar to Fig.4. Two large doses of electron irradiation were applied in this case, 4.1 C/cm^2 (red curve - cooling only) and 6.3 C/cm^2 (green curve, cooling and warming). In addition, zoomed in 6.3 C/cm^2 curve in Fig.5(b) shows two “minor” hysteresis loops when the sample was cooled to the middle of the transition and then warmed up showing switching between the two branches. This is very characteristic of an irreversible behavior. The question is - what is the origin of the hysteretic resistivity? Structural domains would contribute randomly and it is unclear what kind of domains is formed in a slightly distorted monoclinic phase. It seems that a substantial increase of magnetic anisotropy is responsible for such behavior and the hysteresis is connected to under-cooling and super-heating associated with the 1st order transition. Introduced point-like disorder makes the system

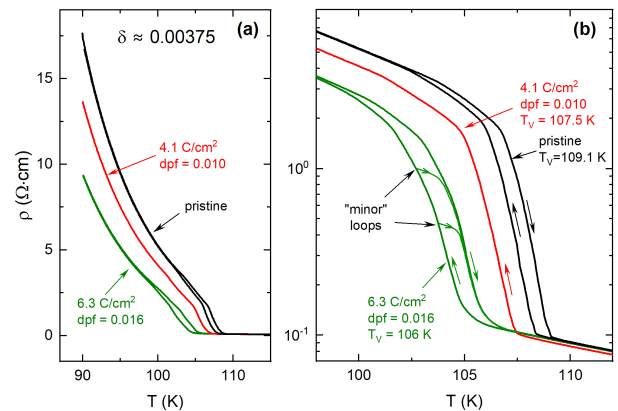


FIG. 5. Measurements similar to Fig.4 performed on an off-stoichiometric magnetite crystal with $T_V \approx 109 \text{ K}$. Two large doses of electron irradiation were applied in this case, 4.1 C/cm^2 (red curve - cooling only) of 10 defects per 1000 formula units and 6.3 C/cm^2 (green curve, cooling and warming) corresponding to 16 defects per 1000 formula units. In addition, zoomed in 6.3 C/cm^2 curve in panel (b) shows two “minor” hysteresis loops when the sample was cooled to the middle of the transition and then warmed up showing switching between the two branches. Quite similar observations may be drawn from this figure as compared to the optimal crystal data of Fig.4.

less perfect and the hysteresis even shrinks somewhat.

We now examine biogenic magnetite extracted from magneto-tactic bacteria. Figure 6 shows transmission electron microscopy (TEM) images of magnetotactic bacteria MV-1 that produce some of the most perfect nanocrystals of magnetite [66, 67, 92]. The extracted magnetite nanocrystals were smeared over the TEM grid and the grid was encapsulated in a thin aluminum foil. This “pack” was measured in *Quantum Design* MPMS before and after irradiation.

Figure 7 shows temperature and field dependent magnetization of magnetite nanocrystals extracted from the MV-1 magnetotactic bacteria. Main panel shows magnetization measured on warming after the sample was cooled to 5 K in zero field, then $H = 500 \text{ Oe}$ magnetic field was applied and the data were collected on warming (this protocol is abbreviated ZFC-W). After reaching maximum temperature, the measurements continued on cooling without turning magnetic field off (FC-C protocol). Pristine sample curve is shown by black filled circles. The curve after electron irradiation of 2 C/cm^2 is shown by open red squares. The inset in Fig.7 shows $T = 5 \text{ K}$ $M(H)$ loops of the same sample, before (dashed black line) and after (solid red line) irradiation. Notice the significant hysteresis between ZFC and FC measurements at all temperatures closing only above 250 K. This means that blocking (collective irreversibility) temperature is somewhere around room temperature [61, 66]. Therefore, the direction of the magnetic moments in mono-domain nanocrystals is fixed ($k_B T_V \ll k_B T_B$), hence the sharp changes around 110 K are due to the Verwey transition.

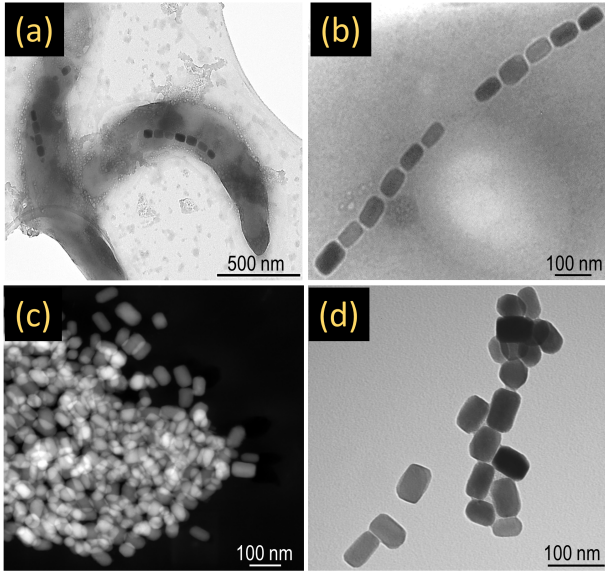


FIG. 6. Biogenic magnetite nanocrystals extracted from MV-1 strain of magnetotactic bacteria. (a) TEM image of the whole bacteria with magnetosome containing a chain of [111] oriented head-to-tail magnetite particles inside. (b) Zoom in on a magnetosome chain. (c) bacteria lysed using French press (d) free magnetite nanoparticles with [111] direction along the long side.

Similar to our observations on crystals described above, Verwey temperature shifts to the lower values and hysteresis becomes somewhat smaller after irradiation.

Finally, we examine the evolution of the Verwey transition temperature with added point-like disorder induced by 2.5 MeV electron irradiation. Figure 8 shows Verwey transition temperature versus off-stoichiometric parameter δ in $\text{Fe}_{3(1-\delta)}\text{O}_4$. The solid lines are the fits to the multiple literature data collected on off-stoichiometric [10, 44–48] and ion-substituted magnetite adjusted to the parameter δ [50–53]. Until now, it is a general belief that for $\delta \lesssim 0.0039$ the transition is of the first order, and can be well approximated by $T_V = 121.3 - 3.2 \times 10^{-3}\delta$, whereas for $\delta \gtrsim 0.0039$ the transition is of the second order and is described by $T_V = 111.4 - 2.5 \times 10^{-3}\delta$. In Fig. 8 our measurements are shown by symbols. Clearly, driven by disorder induced by the electron irradiation, the off-stoichiometric sample enters continuously the “forbidden” range of T_V and shows the same highly hysteretic behavior, against the second order expectations. The hysteresis has also been observed in all previous measurements with no explanation provided of how is this compatible with the 2nd order transition.

IV. DISCUSSION

Our temperature-dependent resistivity measurements in pristine samples are fully consistent with the literature data, so we have a reliable starting point to investi-

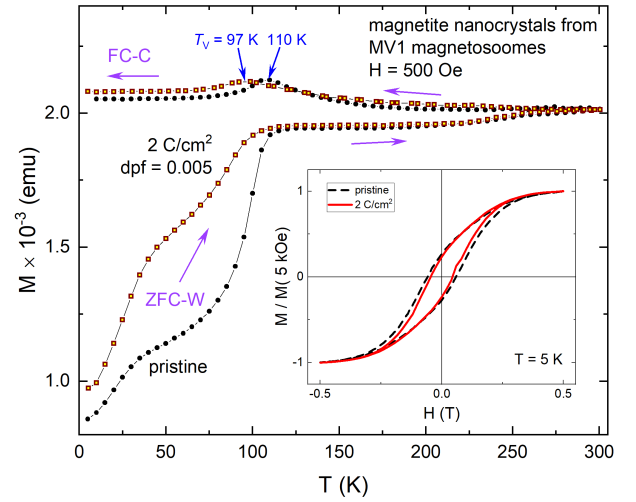


FIG. 7. Magnetic measurements of biogenic magnetite. Main panel shows zero-field cooled (ZFC) measurements, followed by field-cooled (FC) data, both in a $H = 500$ Oe applied magnetic field. Black line is for pristine sample and red after 2 C/cm^2 electron-irradiated sample. The inset shows low-temperature $M(H)$ loops of the same sample at $T = 5$ K before (dashed black line) and after (solid red line) irradiation.

gate the effects of electron irradiation. There are several important features observed in magnetite crystals and nanocrystals before and after electron irradiation that introduces artificial controlled point-like disorder.

(1) The increase of the resistivity above T_V is counter-intuitive, considering activated character of transport. This suggests that carrier mobility is affected stronger by disorder than carrier density.

(2) The sharpness of the step-like $\rho(T)$ transition remains practically unchanged (contrary to the substitutional disorder, which significantly smears and broadens the transition [52]). All curves remain parallel at the transition showing no broadening after the irradiation, they just shift.

(3) The under-cooling / super-heating hysteresis becomes a little bit smaller after irradiation.

(4) Resistivity is not metallic at all temperatures exhibiting semiconductor-like Arrhenius activated behavior with characteristic energy barriers around $U = 200$ meV below T_V and 60 meV above. These values are similar to the reported in literature [41].

(5) These barrier values remain practically unchanged even after substantial increase of the disorder.

(6) The Verwey transition temperature in the irradiated sample shifts by a significant amount of $\Delta T_V / T_V^0 \approx 0.48\%$ per 1 C/cm^2 (6.24×10^{18} electrons/cm 2) in the optimal sample, and 0.45% per 1 C/cm^2 in the lower T_V sample. These are quite similar values despite the large difference in T_V and the actual maximum doses acquired, 3.76 C/cm^2 and 6.3 C/cm^2 , respectively.

(7) The Verwey transition of the lower- T_V sample in pristine state is at the border of an alleged cross-over from the 1st order to the 2nd order transition. The irradi-

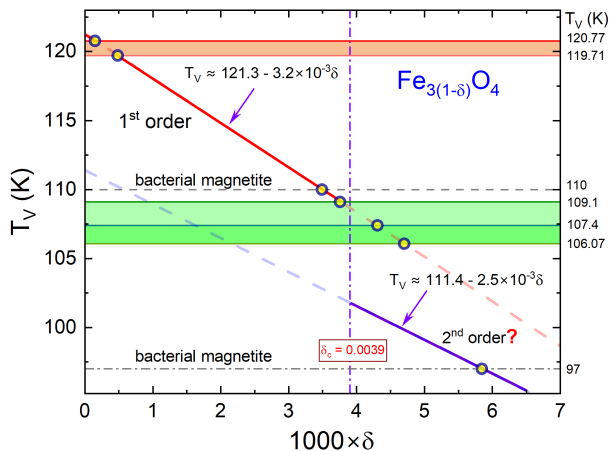


FIG. 8. Verwey transition temperature versus off-stoichiometric parameter, δ , in $\text{Fe}_{3(1-\delta)}\text{O}_4$. The solid lines are the fits to the multiple literature data collected on off-stoichiometric [10, 44–48] and ion-substituted magnetite adjusted to the parameter δ [50–53]. For $\delta \lesssim 0.0039$ the transition is of the first order and is well approximated by $T_V = 121.3 - 3.2 \times 10^{-3} \delta$, whereas for $\delta \gtrsim 0.0039$ the transition was thought to be of the 2nd order and is described by $T_V = 111.4 - 2.5 \times 10^{-3} \delta$. Our measurements are shown by symbols. Importantly, driven by irradiation, the off-stoichiometric sample enters continuously the forbidden range of T_V and shows the same highly hysteretic behavior, against the second order expectations.

ation, however, pushes Verwey temperature continuously to lower values without broadening or smearing and with a substantial hysteresis. This, combined with the original Honig’s observations of such hysteresis means that the discontinuity in the $T_V(\delta)$ or $T_V(\text{doping})$ is most likely due to sample inhomogeneity and phase separation rather than the intrinsic behavior.

(8) Irradiated samples can be annealed toward the pristine state showing the behavior expected for the lower-dose irradiation.

(9) Magnetite nanocrystals extracted from MV-1 strain of magnetotactic bacteria show behavior qualitatively similar to the bulk crystals. The Verwey temperature is suppressed and hysteresis becomes smaller. Of course, it was only possible to measure magnetization, not electric transport.

Is it possible to understand all those features from a single point of view? If the Verwey transition was driven by $\text{Fe}^{2+}/\text{Fe}^{3+}$ ordering and/or electrons/polarons localization, it would be significantly smeared by the additional randomly distributed defects. Also, resistivity would increase at all temperatures. The same arguments can be used against the Wigner glass to crystal transition. In our view, the opening of the band-gap the most plausible explanation of the Verwey transition. Additional disorder, at our low concentrations, does not affect the energy gap itself, but could form an impurity (disorder) band close to the conduction band. Additionally, it would certainly affect/increase the bandwidth

making the band edge “fuzzy”. According to the theory, this would lower the effective activation barrier [93], thus leading to the reduction of T_V . Furthermore, the increase of ρ above T_V , and the decrease below is most likely due to the magnetic component of the problem. At least some irradiation-induced defects may become “magnetic” scatterers when both the defect’s and scattered electron’s spins flip. This would be effective in the magnetically mildly anisotropic cubic phase above T_V but then become less significant in the higher anisotropy monoclinic phase. However, the reason that resistivity decreases in the low-temperature phase after irradiation is the same broadening of the bandwidth lowering the effective barrier, hence leading to more carriers in the conduction band. Apparently this effect dominates the opposed trend of increased density of scattering centers.

V. CONCLUSIONS

To summarize, a 2.5 MeV low-temperature (20 K) electron irradiation was used to induce point-like defects in magnetite crystals and biogenic nanocrystals. The Verwey transition shifts to the lower temperatures regardless of the T_V itself, approximately at the rate of $\Delta T_V/T_V^0 \approx 0.5\%$ per 1 C/cm^2 (6.24×10^{18} electrons/ cm^2). The transition itself remains sharp without any sign of smearing or broadening. In $T_V = 109.1 \text{ K}$ sample, in the pristine state, it is right at the “border” of the alleged 1st-to-2nd order transition. Upon irradiation, the resistivity curve parallel-shifts to what so far was believed to be a “forbidden” range for the Verwey’s T_V . Notably, the transition itself remains sharp and hysteretic arguing against the intrinsic mechanism of the *apparent* 2nd order transition. The wealth of obtained results can be explained within the bandwidth bandgap theory with a smaller gap, around 60 meV above T_V , and a larger gap around 200 meV below T_V . We hope that the obtained data will motivate further work on the mechanisms of the fascinating Verwey transition in magnetite.

ACKNOWLEDGMENTS

We are grateful to Jurgen M. Honig (passed away on November 4, 2022) and to Robert J. McQueeney for illuminating discussions and for providing high-quality single crystals of magnetite; and to Dennis A. Bazylinski for valuable discussions and providing biogenic nanocrystals from the MV-1 magnetotactic bacteria.

This research was supported by the U.S. Department of Energy (DOE), Office of Science, Basic Energy Sciences, Materials Science and Engineering Division. Ames Laboratory is operated for the U.S. DOE by Iowa State University under contract DE-AC02-07CH11358. We thank the SIRIUS team for running electron irradiation at École Polytechnique supported by the EMIR&A (the French Federation of Accelerators for Irradiation and Analysis

-
- [1] G. S. Parks and K. K. Kelley, *J. Phys. Chem.* **30**, 47 (1926).
- [2] E. J. W. Verwey, *Nature* **144**, 327 (1939).
- [3] E. Verwey and P. Haayman, *Physica* **8**, 979 (1941).
- [4] H. Liu and C. D. Valentin, *The Journal of Physical Chemistry C* **121**, 25736 (2017).
- [5] P. Weiss and R. Forrer, *Annales de physique* **10**, 279 (1929).
- [6] C. H. Li, *Physical Review* **40**, 1002 (1932).
- [7] L. R. Bickford, *Reviews of Modern Physics* **25**, 75 (1953).
- [8] R. A. Buckwald, A. A. Hirsch, D. Cabib, and E. Callen, *Phys. Rev. Lett.* **35**, 878 (1975).
- [9] Review, *Philos. Mag. B* **42**, 325 (1980).
- [10] J. M. Honig, *Journal Of Alloys And Compounds* **229**, 24 (1995).
- [11] A. R. Muxworthy and E. McClelland, *Geophysical Journal International* **140**, 101 (2000).
- [12] M. J. Jackson and B. Moskwitz, *Geophysical Journal International* **224**, 1314 (2020).
- [13] W. Friedrich, *Journal of Physics: Condensed Matter* **14**, R285 (2002).
- [14] J. García and G. Subías, *Journal of Physics: Condensed Matter* **16**, R145 (2004).
- [15] D. A. Bazylinski and R. B. Frankel, *Nature Reviews Microbiology* **2**, 217 (2004).
- [16] G. K. Rozenberg, M. P. Pasternak, W. M. Xu, Y. Amiel, M. Hanfland, M. Amboage, R. D. Taylor, and R. Jeanloz, *Phys. Rev. Lett.* **96**, 045705 (2006).
- [17] R. S. Coe, R. Egli, S. A. Gilder, and J. P. Wright, *Earth and Planetary Science Letters* **319-320**, 207 (2012).
- [18] Q. Yu, A. Mottaghizadeh, H. Wang, C. Ulysse, A. Zimmers, V. Rebutini, N. Pinna, and H. Aubin, *Phys. Rev. B* **90**, 075122 (2014).
- [19] I. Bernal-Villamil and S. Gallego, *Journal Of Physics-condensed Matter* **27**, 293202 (2015).
- [20] J. de la Figuera and J. F. Marco, *Hyperfine Interactions* **240**, 44 (2019), 16th Latin American Conference on the Applications of the Mossbauer Effect (LACAME), Santiago de Chile, Chile, Nov 18-23, 2018.
- [21] S. S. Aplesnin and G. I. Barinov, *Phys. Solid State* **49**, 1949 (2007).
- [22] G. Subías, J. García, J. Blasco, M. Grazia Proietti, H. Renevier, and M. Concepción Sánchez, *Phys. Rev. Lett.* **93**, 156408 (2004).
- [23] P. Anderson, *Phys. Rev.* **102**, 1008 (1956).
- [24] N. Mott, *Metal-Insulator Transitions* (CRC Press, 2004).
- [25] T. E. Whall, M. O. Rigo, M. R. B. Jones, and A. J. Pointon, *Journal de Physique Colloques* **38**, C1 (1977).
- [26] T. E. Whall, *Philosophical Magazine B* **42**, 423 (1980).
- [27] M. S. Senn, J. P. Wright, and J. P. Attfield, *Nature* **481**, 173 (2011).
- [28] M. S. Senn, J. P. Wright, J. Cumby, and J. P. Attfield, *Phys. Rev. B* **92**, 024104 (2015).
- [29] H. Y. Huang, Z. Y. Chen, R. P. Wang, F. M. F. de Groot, W. B. Wu, J. Okamoto, A. Chainani, A. Singh, Z. Y. Li, J. S. Zhou, H. T. Jeng, G. Y. Guo, J.-G. Park, L. H. Tjeng, C. T. Chen, and D. J. Huang, *Nature Communications* **8**, 15929 (2017).
- [30] S. de Jong, R. Kukreja, C. Trabant, N. Pontius, C. F. Chang, T. Kachel, M. Beye, F. Sorgenfrei, C. H. Back, B. Bräuer, W. F. Schlotter, J. J. Turner, O. Krupin, M. Doehler, D. Zhu, M. A. Hossain, A. O. Scherz, D. Fausti, F. Novelli, M. Esposito, W. S. Lee, Y. D. Chuang, D. H. Lu, R. G. Moore, M. Yi, M. Trigo, P. Kirchmann, L. Pathey, M. S. Golden, M. Buchholz, P. Metcalf, F. Parmigiani, W. Wurth, A. Föhlisch, C. Schübler-Langeheine, and H. A. Dürr, *Nature Materials* **12**, 882 (2013).
- [31] W. Wang, J. Li, Z. Liang, L. Wu, P. M. Lozano, A. C. Komarek, X. Shen, A. H. Reid, X. Wang, Q. Li, W. Yin, K. Sun, Y. Zhu, I. K. Robinson, M. P. M. Dean, and J. Tao, *arXiv:2202.08744* (2022).
- [32] A. Bosak, D. Chernyshov, M. Hoesch, P. Piekarczyk, M. Le Tacon, M. Krisch, A. Kozłowski, A. M. Oleś, and K. Parlinski, *Phys. Rev. X* **4**, 011040 (2014).
- [33] B. Chakraverty, *Solid State Communications* **15**, 1271 (1974).
- [34] H. P. Pinto and S. D. Elliott, *Journal of Physics: Condensed Matter* **18**, 10427 (2006).
- [35] M. O. Rigo and J. Kleinclauss, *Philosophical Magazine B* **42**, 393 (1980).
- [36] Y. Yamada, *Philosophical Magazine B* **42**, 377 (1980).
- [37] N. F. Mott, *Adv. S. S. Phys, Festkorperprobleme* **19**, 331 (1979).
- [38] N. F. Mott, *Philosophical Magazine B* **42**, 327 (1980).
- [39] C. M. Srivastava, *Phys. Lett. A* **98A**, 192 (1983).
- [40] E. I. Terukov, W. Reichelt, D. Ihle, and H. Oppermann, *Physica Status Solidi (b)* **95**, 491 (1979).
- [41] A. Banerjee and A. J. Pal, *Journal Of Physics-condensed Matter* **32**, 055701 (2020).
- [42] D. Ihle and B. Lorenz, *Philosophical Magazine B* **42**, 337 (1980).
- [43] H.-T. Jeng, G. Y. Guo, and D. J. Huang, *Phys. Rev. Lett.* **93**, 156403 (2004).
- [44] R. Aragon, J. P. Shepherd, J. W. Koenitzer, D. J. Buttrely, R. J. Rasmussen, and J. M. Honig, *J. Appl. Phys.* **57**, 3221 (1985).
- [45] Z. Kakol and J. M. Honig, *Solid State Commun.* **70**, 967 (1989).
- [46] J. M. Honig, *Proc. - Indian Acad. Sci., Chem. Sci.* **96**, 391 (1986).
- [47] G. K. Rozenberg, G. R. Hearne, M. P. Pasternak, P. A. Metcalf, and J. M. Honig, *Phys. Rev. B* **53**, 6482 (1996).
- [48] J. P. Shepherd, J. W. Koenitzer, R. Aragon, J. Spalek, and J. M. Honig, *Phys. Rev. B: Condens. Matter* **43**, 8461 (1991).
- [49] J. M. Honig, J. Spalek, and P. Gopalan, *J. Am. Ceram. Soc.* **73**, 3225 (1990).
- [50] C. Djega-Mariadassou, T. Merceron, J. L. Dormann, M. Porte, and P. Renaudin, *Phys. Status Solidi A* **112**, 601 (1989).
- [51] Z. Kakol, J. Sabol, J. Stickler, and J. M. Honig, *Phys. Rev. B: Condens. Matter* **46**, 1975 (1992).
- [52] V. A. M. Brabers, F. Walz, and H. Kronmüller, *Phys. Rev. B: Condens. Matter Mater. Phys.* **58**, 14163 (1998).
- [53] L. Gasparov, A. Rush, T. Pekarek, N. Patel, and

- H. Berger, *J. Appl. Phys.* **105**, 07E109 (2009).
- [54] Y. Kakudate, N. Mori, and Y. Kino, *Journal of Magnetism and Magnetic Materials* **12**, 22 (1979).
- [55] N. Mori, S. Todo, N. Takeshita, T. Mori, and Y. Akishige, *Physica B - Condensed Matter* **312**, 686 (2002), international Conference on Strongly Correlated Electron Systems (SCES 01), Ann Arbor, MI, Aug 06-10, 2001.
- [56] L. Gasparov, Z. Shirshikova, T. M. Pekarek, J. Blackburn, V. Struzhkin, A. Gavriluk, R. Rueckamp, and H. Berger, *J. Appl. Phys.* **112**, 043510 (2012).
- [57] Y. Nagasawa, M. Kosaka, S. Katano, N. Mori, S. Todo, and Y. Uwatoko, *Journal Of The Physical Society Of Japan* **76**, 110 (2007).
- [58] G. F. Goya, T. S. Berquo, F. C. Fonseca, and M. P. Morales, *J. Appl. Phys.* **94**, 3520 (2003).
- [59] J. E. Lima, A. L. Brandl, A. D. Arelaro, and G. F. Goya, *J. Appl. Phys.* **99**, 083908 (2006).
- [60] A. Mitra, J. Mohapatra, S. S. Meena, C. V. Tomy, and M. Aslam, *J. Phys. Chem. C* **118**, 19356 (2014).
- [61] R. Prozorov, Y. Yeshurun, T. Prozorov, and A. Gedanken, *Phys. Rev. B* **59**, 6956 (1999).
- [62] J. Wang, Q. Chen, X. Li, L. Shi, Z. Peng, and C. Zeng, *Chemical Physics Letters* **390**, 55 (2004).
- [63] J. B. Yang, X. D. Zhou, W. B. Yelon, W. J. James, Q. Cai, K. V. Gopalakrishnan, S. K. Malik, X. C. Sun, and D. E. Nikles, *J. Appl. Phys.* **95**, 7540 (2004).
- [64] W. Kim, C.-Y. Suh, S.-W. Cho, K.-M. Roh, H. Kwon, K. Song, and I.-J. Shon, *Talanta* **94**, 348 (2012).
- [65] F. C. Meldrum, S. Mann, B. R. Heywood, R. B. Frankel, and D. A. Bazylinski, *Proceedings: Biological Sciences* **251**, 231 (1993).
- [66] R. Prozorov, T. Prozorov, S. K. Mallapragada, B. Narasimhan, T. J. Williams, and D. A. Bazylinski, *Phys. Rev. B* **76**, 054406 (2007).
- [67] R. E. Dunin-Borkowski, *Science* **282**, 1868 (1998).
- [68] E. T. Simpson, T. Kasama, M. Posfai, P. R. Buseck, R. J. Harrison, and R. E. Dunin-Borkowski, *Journal of Physics: Conference Series* **17**, 108 (2005).
- [69] D. L. Sage, K. Arai, D. R. Glenn, S. J. DeVience, L. M. Pham, L. Rahn-Lee, M. D. Lukin, A. Yacoby, A. Komeili, and R. L. Walsworth, *Nature* **496**, 486 (2013).
- [70] J. Lee, S. G. Kwon, J.-G. Park, and T. Hyeon, *Nano Lett.* **15**, 4337 (2015).
- [71] R. Prozorov and T. Prozorov, *J. Mag. Mag. Mater.* **281**, 312 (2004).
- [72] R. Prozorov, M. Kończykowski, M. A. Tanatar, H.-H. Wen, R. M. Fernandes, and P. C. Canfield, *npj Quantum Materials* **4**, 34 (2019).
- [73] J. Brabers, F. Walz, and H. Kronmuller, *Physica B* **266**, 321 (1999).
- [74] F. Rullier-Albenque, P. A. Vieillefond, H. Alloul, A. W. Tyler, P. Lejay, and J. F. Marucco, *Europhysics Letters (EPL)* **50**, 81 (2000).
- [75] A. C. Damask and G. J. Dienes, *Point Defects in Metals* (Gordon & Breach Science Publishers Ltd, 1963).
- [76] M. W. Thompson, *Defects and Radiation Damage in Metals*, revised september 27, 1974 ed., Cambridge Monographs on Physics (Cambridge University Press, 1969).
- [77] R. Prozorov, M. Kończykowski, M. A. Tanatar, A. Thaler, S. L. Bud'ko, P. C. Canfield, V. Mishra, and P. J. Hirschfeld, *Phys. Rev. X* **4**, 041032 (2014).
- [78] K. Cho, M. Kończykowski, S. Teknowijoyo, M. A. Tanatar, and R. Prozorov, *Supercond. Sci. Technol.* **31**, 064002 (2018).
- [79] K. Cho, M. Kończykowski, S. Teknowijoyo, M. A. Tanatar, J. Guss, P. B. Gartin, J. M. Wilde, A. Kreyssig, R. J. McQueeney, A. I. Goldman, V. Mishra, P. J. Hirschfeld, and R. Prozorov, *Nat. Commun.* **9**, 2796 (2018).
- [80] The SIRIUS linear accelerator: <https://portail.polytechnique.edu/lsi/en/facilities/sirius-installation> (1960).
- [81] O. S. Oen, *Cross sections for atomic displacements in solids by fast electrons* (Office of Scientific and Technical Information (OSTI), ID: 4457758, Report: ORNL-4897, 1973).
- [82] H. R. Harrison, R. Aragón, J. E. Keem, J. M. Honig, and J. F. Wenckus, in *Inorganic Syntheses*, Vol. 22 (John Wiley & Sons, Inc. (2007), 1983) pp. 43–48.
- [83] M. A. Tanatar, A. E. Böhmer, E. I. Timmons, M. Schütt, G. Drachuck, V. Taufour, K. Kothapalli, A. Kreyssig, S. L. Bud'ko, P. C. Canfield, R. M. Fernandes, and R. Prozorov, *Phys. Rev. Lett.* **117**, 127001 (2016).
- [84] E. I. Timmons, S. Teknowijoyo, M. Kończykowski, O. Cavani, M. A. Tanatar, S. Ghimire, K. Cho, Y. Lee, L. Ke, N. H. Jo, S. L. Bud'ko, P. C. Canfield, P. P. Orth, M. S. Scheurer, and R. Prozorov, *Phys. Rev. Res.* **2**, 023140 (2020).
- [85] D. A. Bazylinski, R. B. Frankel, and H. W. Jannasch, *Nature* **334**, 518 (1988).
- [86] R. P. Blakemore, *Science* **190**, 377 (1975).
- [87] R. B. Frankel, R. P. Blakemore, and R. S. Wolfe, *Science* **203**, 1355 (1979).
- [88] L. Degiorgi, I. Blatter-Moerke, and P. Wachter, *Phys. Rev. B: Condens. Matter* **35**, 5421 (1987).
- [89] P. A. Miles, W. B. Westphal, and A. Von Hippel, *Rev. Mod. Phys.* **29**, 279 (1957).
- [90] J. R. Cullen and E. Callen, *J. Phys. (Paris)* **32**, 1110 (1971).
- [91] D. L. Camphausen and B. K. Chakraverty, in *Proceedings of the 11th International Conference on the Physics of Semiconductors* (Polish Scientific Publishers, Warsaw, 1972) p. 1266.
- [92] B. L. Dobbels, A. A. DiSpirito, J. D. Morton, J. D. Semrau, J. N. Neto, and D. A. Bazylinski, *Microbiology* **150**, 2931 (2004).
- [93] J. H. V. J. Brabers, F. Walz, and H. Kronmuller, *J. Phys.: Condens. Matter* **12**, 5437 (2000).